



## Biofuel Production from Palm Oil Mill Effluent through Hydrocracking Using Natural Zeolite-Supported Transition Metal Oxide Catalyst

Gimelliya Saragih<sup>a\*</sup>, Harmileni<sup>a</sup>, Junifa Layla Sihombing<sup>b</sup>, and Ahmad Nasir Pulungan<sup>b</sup>

<sup>a</sup>Politeknik Teknologi Kimia Industri, Medan 20228, Indonesia

<sup>b</sup>Department of Chemistry, Faculty of Mathematics and Natural Sciences, Universitas Negeri Medan, Jl. Willem Iskandar Pasar V Medan Estate, Medan 20221, Indonesia



### Abstract

Palm oil mill effluent (POME) is a liquid waste from the processing of crude palm oil (CPO) which has not been utilized optimally. Oil extraction from POME resulted in an oil yield of 9923 mg/L. The residual oil from POME can be converted into fuel through catalytic hydrocracking with heterogeneous catalysts such as zeolite. The natural zeolite catalyst used in this research is Sarulla natural zeolite (SNZ) from North Sumatera, Indonesia. SNZ was activated with mineral acids and then loaded with PbO and ZnO metal oxides. The surface morphology of the catalysts was quite homogeneous with fine particle sizes of 1-2  $\mu\text{m}$ . The surface areas of PbO/SNZ and ZnO/SNZ catalysts were 81.9 and 58.5  $\text{m}^2/\text{g}$ , with pore diameters of 3.09 and 3.58 nm, respectively. The obtained biofuel has a conversion to the liquid product of 40-44% obtained from POME catalyzed with a mass catalyst of 0.15 wt.%. The liquid product catalyzed by PbO/SNZ was more selective towards the gasoline fraction with a selectivity of 22-30%. Meanwhile, ZnO/SNZ 0.15 wt.% catalyzed produced more kerosene fraction with the highest selectivity of 52%. The highest HHV of biofuel (44.2 MJ/kg) was obtained from the liquid product catalyzed by ZnO/SNZ 0.12 wt.%.

**Keywords:** Biofuel; catalytic hydrocracking; palm oil mill effluent; natural zeolite catalyst

### 1. Introduction

Production of crude palm oil (CPO) in Indonesia is the largest in the world. In 2021, it was reported that Indonesia produced CPO reaching 46 million tons and is expected to continue to increase in 2022 to reach 49 million tons (Gapki, 2021). The increase in CPO production is directly proportional to the waste produced, including empty fruit bunches, fibre, shells, ash, and liquid waste called Palm oil mill effluent (POME) [1-5]. In 2012 there were 60-83 million tons of liquid waste then this number increased by 85-110 million tons until 2020 [6]. To increasing the value of this liquid waste, many studies have been carried out on the use of POME in various fields, including as a medium for microalgae growth [7,8] because it has high levels of COD and BOD, besides that POME can be applied as a source

of biogas [9], as well as liquid fuel [10]. Moreover, POME waste can be a potential source of raw materials for biofuel production because it contains oil ranging from 4000-8000 mg/L [11-14]. The potential of this POME waste has not been widely used at this time as an alternative fuel source, even though the residual content of this vegetable oil can be converted into environmentally friendly fuel through the hydrocracking process.

Several studies have carried out the process of hydrocracking vegetable oil into fuel [15-18]. These results indicate that the main content of triglycerides and fatty acids can be converted into biofuels, both gasoline, kerosene, and diesel fractions. In hydrocracking a catalyst is needed to speed up the reaction. Several types of catalysts have been used for the production of biofuels from vegetable oils,

\*Corresponding author e-mail: [gimelliya.s@gmail.com](mailto:gimelliya.s@gmail.com); (Gimelliya Saragih).

EJCHEM use only; Received date 16 December 2022; revised date 15 March 2023; accepted date 10 April 2023

DOI: 10.21608/EJCHEM.2023.180971.7340

©2023 National Information and Documentation Center (NIDOC)

including Alumina [19,20], clay [21,22], and zeolite [23,24]. However, until now, zeolites are the most important catalysts in the petrochemical industry because of their excellent chemical properties, namely acidity, good thermal stability at high temperatures and having large pores that allow the reactants to access the surface [25]. In addition, to improve the catalytic performance of the catalyst, the zeolite material can be combined with transition metal oxide (TMO) such as PbO and ZnO. The use of TMO has been widely developed because of its good catalytic activity and low price which can reduce production costs [26]. Hasanudin et al. [27] have carried out an esterification reaction of free fatty acids (FFA) from POME samples using a sulfonated carbon-zeolite composite catalyst, producing FAME products of 93.75%. Another study by Muanruksa et al. [28] have converted POME into biofuel through enzymatic hydrolysis and decarboxylation resulted in the refined-biofuel yield (94%) and the biojet selectivity (57.44%). But so far, the use of natural zeolite as a catalyst to convert palm oil liquid waste as fuel is still limited, even though the availability of natural zeolite is very abundant, especially in Indonesia. Thus, POME processing and the use of natural zeolite from Sarulla village are expected to increase the economic value of fuel that can be used by the community and industry.

In this study, the conversion process of POME waste into liquid fuel is carried out through a catalytic hydrocracking process in a fixed bed system reactor using a natural zeolite Sarulla catalyst sourced from North Sumatera, Indonesia. This zeolite was treated with transition metal oxides ZnO and PbO to increase the total conversion and product selectivity towards the biofuel fraction.

## 2. Experimental

Palm oil mill effluent (POME) was obtained from the PTKI Medan mini palm oil mill. Distilled water, double distilled water (DDW), natural zeolite from Sarulla (North Sumatera, Indonesia).  $Zn(NO_3)_2 \cdot 4H_2O$  (p.a),  $Pb(NO_3)_2$  (p.a), HCl,  $HNO_3$ ,  $H_2SO_4$ ,  $H_3PO_4$  (p.a), n-hexane, methanol (p.a), NaOH (p.a.) from Merck (Darmstadt, Germany). Hydrogen, oxygen and nitrogen gases from PT. Aneka Gas (Medan, Indonesia).

### 2.1 Palm Oil Mill Effluent Preparation

POME is heated at 105 °C to evaporate the water, then filtered to separate the mixed solids. Phosphatides, proteins and resins are separated by degumming, namely by adding a solution of phosphoric acid ( $H_3PO_4$  0.6%), as much as 1-3% of the volume of palm oil liquid waste.

The oil-fat extraction process was carried out using n-hexane as solvent. The ratio of n-hexane:POME is 1:0.8. The mixture was then sonicated for 5 min and transferred to a separatory funnel, allowed to separate into two layers for 15 min. The top layer was evaporated to obtain a thick oil extract from POME. The viscous extract obtained was heated at 105 °C for 45 minutes to remove the remaining solvent. After drying, the oil is placed in a desiccator, and the oil recovery is calculated using equation (1).

$$\text{Yield (mg/L)} = \frac{\text{Weight Dry Oil Content (mg)} \times 1000}{\text{Sample Volume (L)}} \quad (1)$$

### 2.2 Preparation and Activation of Sarulla Natural Zeolite

The preparation and activation of natural zeolite in this study followed the procedure reported by Sihombing et al. [15]. At the initial stage, natural zeolite was crushed and sieved to obtain zeolite with a size that passes through a 100 mesh sieve. The natural zeolite was then washed by immersion in distilled water for 24 h at room temperature, then filtered and dried at 100 °C. The zeolite was then activated using 3M HCl at 90 °C for 30 min. The sample was filtered, the precipitate was washed using distilled water until the pH was neutral, the precipitate was filtered and then dried at 120 °C for 3 h. The sample was calcined at 500 °C with  $N_2$  gas flow to obtain acid activated Sarulla natural zeolite (SNZ).

### 2.3 Preparation of ZnO/SNZ and PbO/SNZ Catalysts

TMO loaded on natural zeolite Sarulla was carried out following the procedure reported by Pulungan et al. [26] with the wet impregnation method followed by the oxidation process. In the initial stage, an amount of  $Zn(NO_3)_2 \cdot 4H_2O$  dissolved in DDW then added SNZ in a certain ratio, put into a three-neck flask and heated at 90 °C for 4 h. The mixture was dried at 130 °C, followed by a calcination process at 500 °C for 1 h with  $N_2$  gas flow, then oxidized at the same temperature with gas  $O_2$  for 1 h to obtain a ZnO/SNZ catalyst. The same

steps were carried out for the preparation of PbO/SNZ catalysts.

#### 2.4 Catalyst Characterization

The crystallinity properties of the catalyst are analyzed by X-Ray Diffractometer (XRD Shimadzu 6100) Cu K $\alpha$  ( $\lambda = 1.54184$ ) radiation at 40kV and 30 mA in the area  $2\theta = 7.00\text{--}70.00^\circ$ . The catalyst's surface morphology, elemental analysis, and mapping are analyzed using a Zeiss EPOMH 10Zss SEM equipped with Energy Dispersion X-Ray Spectroscopy (EDX). The nitrogen gas adsorption-desorption isotherm analysis is carried out with the Gas Sorption Analyzer (NOVA 1200e) Quantachrome instrument at 77 K. The specific surface area is analyzed by the Brunauer-Emmett-Teller (BET) method. Meanwhile, the volume and pore diameter is based on the Barrett-Joyner-Halenda (BJH) model.

#### 2.5 Hydrocracking Process

The hydrocracking process is carried out using a fixed bed system reactor. The reactor where the reaction takes place has a diameter of 5.5 cm with a height of 25 cm, a catalyst vessel with a diameter of 4.8 cm and a height of 3.5 cm, while the furnace has a diameter of 40 cm and a height of 39 cm.

Oil extracted from POME and catalyst with masses of 0.09, 0.12, and 0.15 wt.% were heated at 500 °C in a heating flask which had been set with temperature control for 2 h. The oil vapor that has been cracked by the catalyst is then cooled, so that the steam is condensed. The reaction was stopped when the composition of the oil in the heating flask was exhausted or no longer emitted liquid vapor. The condensed liquid is then accommodated for analysis using Gas Chromatography Mass Spectrophotometry (GC-MS) to determine the carbon chain and the type of biofuel produced. To determine the higher heating value (HHV) of the fuel, an analysis was carried out using a Bomb Calorimeter.

### 3. Results and Discussion

#### 3.1 Palm Oil Mill Effluent Preparation

Oil extraction was carried out according to the gravimetric method (APHA standard 5520 B). The technique of separating constituents based on their relative solubility is known as solvent extraction. N-hexane is used as an organic solvent because it has the highest oil extraction efficiency and is widely

used in the vegetable oil sector [29]. The extracted residual oil yield was 9923 mg/L.

The oil extracted from POME was analyzed using Gas Chromatography (GC), this analysis aims to determine the compounds contained in the oil extraction sample from POME. GC analysis data of oil extract from POME are summarized in Table 1.

**Table 1**

Fatty acid components contained in the oil extracted from POME

Fatty acid name	Component (%)
Caprylic acid (C8)	0.16
Capric acid	0.17
Lauric acid	2.47
Myristic acid	1.7
Pentadecyclic acid	0.04
Palmitic acid	39.57
Marcaric acid	0.08
Stearic acid	4.67
Oleic acid	38.45
Linoleic acid	10.82
Linolenic acid	0.22
Arachidic acid	0.34
Behenic acid	0.04

The results of the analysis showed that POME oil extract contained various types of fatty acids. The main fatty acids contained include lauric acid (C12) 2.47%, myristic acid (C14) 1.7%, palmitic acid (C16) 39.57%, stearic acid (C18) 4.67%, oleic acid (C18:1C-1) 38.45 %, and linoleic acid (C18:2C) 10.82 %.

#### 3.2 Analysis of Catalyst Crystallinity

The crystallinity analysis of the catalyst was carried out with an XRD instrument. XRD is an analytical technique used to identify phases and characterize crystalline materials based on their diffraction patterns. The results of XRD analysis of samples from PbO/SNZ, and ZnO/SNZ catalysts can be seen in Figure 1.

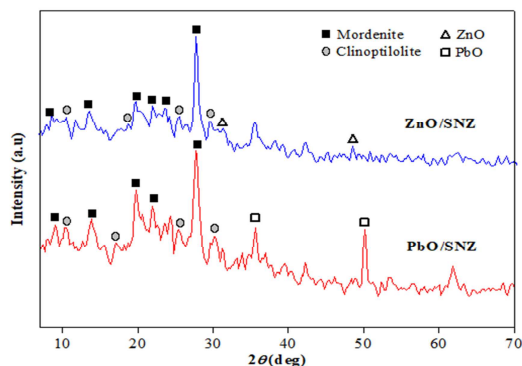


**Figure 1:** XRD diffractogram of PbO/SNZ and ZnO/SNZ catalysts

Based on the diffractogram above, peak characteristics for natural zeolite are observed in the range of  $2\theta = 9\text{--}30^\circ$ . In both diffractogram patterns, several peaks appearing at  $9.9^\circ$ ,  $13.6^\circ$ ,  $19.6^\circ$ ,  $22.4^\circ$ ,  $25.6^\circ$ , and  $27.7^\circ$  are characteristic of mordenite (JCPDS file 5–0490). Meanwhile, the peaks observed at  $11.2^\circ$ ,  $17.3^\circ$ ,  $26.3^\circ$ , and  $30.0^\circ$  fit with the corresponding data of *clinoptilolite* (JCPDS file 25–1349) [30]. This proves that the types of minerals contained in the natural zeolite used are mordenite and *clinoptilolite*. In addition, typical peaks for TMO were also observed. PbO appears at  $2\theta = 37.2^\circ$  and  $50.8^\circ$  (JCPDS No. 76-1796) [31]. While ZnO appears at  $2\theta = 31.4^\circ$  and  $48.3^\circ$  (JCPDS File 89-0510). The characteristic peaks that appear on the diffractograms of both catalysts generally show the same diffraction pattern. This indicates that the treatment of zeolite bearing with metal oxides does not damage the crystal structure of the zeolite and still shows good crystallinity.

### 3.3 Analysis of Catalyst Surface Morphology

The surface morphology of the catalyst was analyzed using SEM with a magnification of 3000 times (Figure 2). Based on the morphological imaging of the catalyst in Figure 2, the ZnO/SNZ catalyst showed a more homogeneous surface with a relatively smaller particle size than PbO/SNZ catalysts. On the other hand, the PbO/SNZ catalyst showed a larger particle size due to agglomeration. This may occur due to metal agglomeration attached to the zeolite surface making the particles form larger aggregates. This is also supported by the particle size distribution analysis carried out on both catalysts. ZnO/SNZ catalyst shows a narrower and more homogeneous particle distribution in the 1–2  $\mu\text{m}$  range, while the PbO/SNZ catalyst has a wider dominant particle size in the 1–3  $\mu\text{m}$  range.

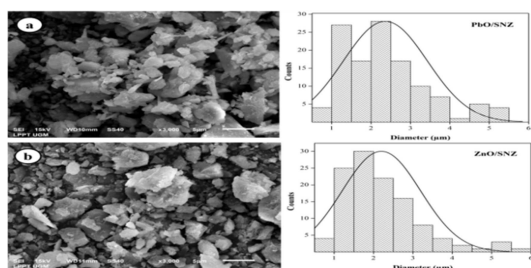


**Figure 2:** Surface morphology and particle size distribution of (a) PbO/SNZ and (b) ZnO/SNZ catalysts

### 3.4 Catalyst Composition

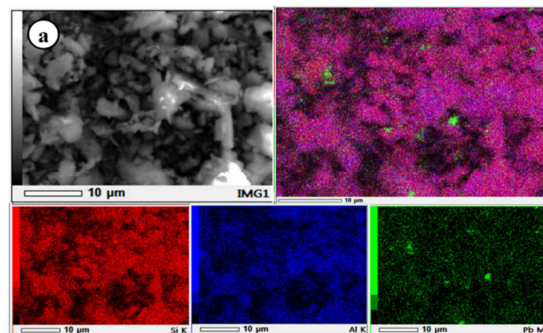
The components contained in the catalyst were analyzed by EDX and summarized in Table 2. Based on previous research by Gea et al. [21] SNZ contains Si, Al and O as the main composition of the zeolite framework. Pb and Zn metals which were not found in SNZ were detected in PbO/SNZ and ZnO/SNZ catalysts of 2.57 and 2.36%, respectively. Moreover, the Si/Al molar ratio increased in PbO/SNZ and ZnO/SNZ catalysts compared to SNZ. The ratio of Si and Al content can affect the characteristics of the catalyst. Catalysts with a greater Si/Al ratio have higher thermal stability [32,33]. As a result, these catalysts are able to maintain their structure at high reaction temperatures. Sequentially the ratio of Si/Al catalyst from the highest is ZnO/SNZ > PbO/SNZ > SNZ.

**Table 2**

Composition and Si/Al ratio of PbO/SNZ and ZnO/SNZ catalyst			
Composition (Mass %)	SNZ <sup>a</sup>	PbO/SNZ	ZnO/SNZ
Si	15.7	20.2	26.0
O	61.6	46.9	52.0
Al	5.64	6.78	8.32
Pb	0.00	2.57	0.00
Zn	0.00	0.00	2.36
Si/Al	2.68	2.86	3.00

<sup>a</sup> Gea et al. [21]

The distribution of the elements in the zeolite can be identified by SEM-Mapping imaging as shown in Figure 3. Each element is represented by a specific color. The darker the color, the more the element is distributed on the surface of the zeolite [34]. This is in accordance with the catalyst composition data by EDX analysis where the larger composition of Si (red) and Al (blue) looks more concentrated, while Pb and Zn metals are represented by a green color which is not too dominant because of their little concentrations.



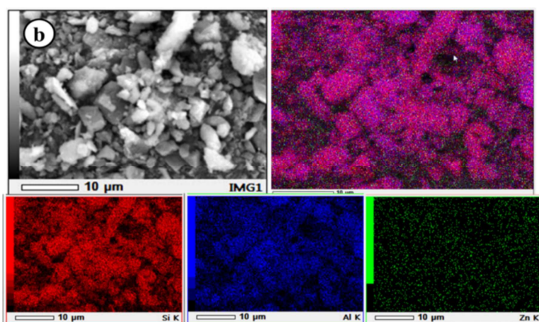


**Figure 3:** Elemental mapping of (a) PbO/SNZ and (b) ZnO/SNZ catalysts

### 3.5 Surface Area and Pore Characteristics of Catalyst

The pore characteristics of the material can be estimated by observing the graphic form of the  $N_2$  gas adsorption-desorption isotherm. The graph of the isotherm for each catalyst can be seen in Figure 4. The presence of a hysteresis loop at a relative pressure of 0.4-0.9 characterizes the type IV isotherm graph based on the IUPAC classification which indicates the presence of mesopores with a pore size of 2-50 nm [35].

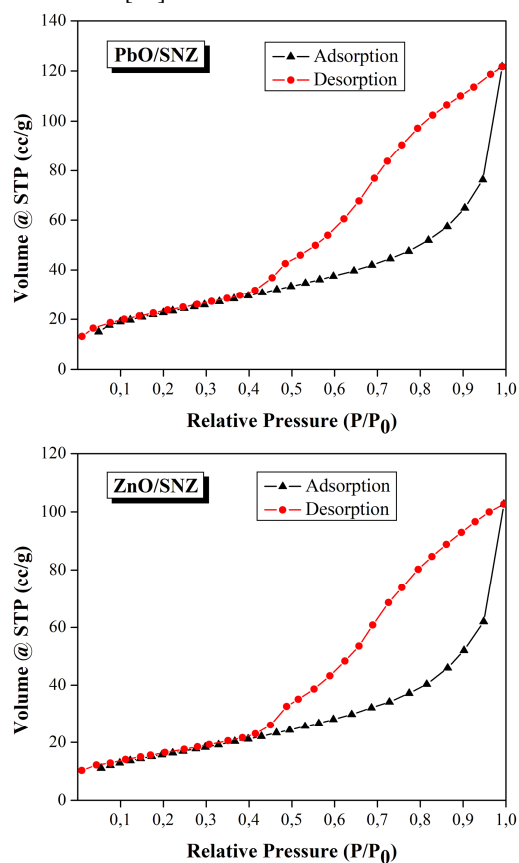


**Figure 4:** Graph of  $N_2$  gas adsorption-desorption isotherm on PbO/SNZ and ZnO/SNZ catalysts

The surface area of the catalyst was analyzed using the Brunauer, Emmett and Teller (BET) method. Meanwhile, the pore diameter and total pore volume were analyzed from the adsorption band using the Barrett, Joyner and Halenda (BJH) method. Data on the surface area and pore characteristics of each catalyst are summarized in Table 3. Referring to the study by Gea et al. [21], in this study, there was a change in the surface area, pore volume and pore diameter of the catalyst after being loaded with metal oxide compared to the initial characteristics of the SNZ catalyst. Based on Table 3, PbO/SNZ catalyst has a surface area of  $81.9 \text{ m}^2/\text{g}$ , which is larger than the surface area of the ZnO/SNZ and SNZ catalyst. In addition, the pore volume of the PbO/SNZ catalyst is also larger ( $0.167 \text{ cc/g}$ ) compared to ZnO/SNZ and SNZ, which are only  $0.147 \text{ cc/g}$  and  $0.150 \text{ cc/g}$ , respectively. However, for the pore size, the ZnO/SNZ catalyst has a wider pore diameter of 3.58 nm, while the pore diameters of PbO/SNZ and SNZ are 3.09 nm and 3.44 nm, respectively. This data is also in accordance with the pore size distribution graph in Figure 5 which shows both catalysts have a pore diameter size that is dominated in the range of  $20\text{-}40 \text{ \AA}$  (2-4 nm). From these data, it can be assumed that ZnO/SNZ has wide but shallow pores, while PbO/SNZ has narrow but deeper pores [34]. The larger surface area can increase the catalytic activity of the catalyst for the reaction on the external surface area. The larger the surface area, the easier the adsorption process to the active site of the catalyst will be. On the other hand, a larger pore diameter is also able to improve the performance of the catalyst in absorbing bulk molecules for further reaction [36,37].

**Table 3**

Surface area, pore volume, and pore diameter of the catalysts

Catalyst	Surface area ( $\text{m}^2/\text{g}$ )	Pore volume ( $\text{cc/g}$ )	Pore diameter (nm)
SNZ <sup>a</sup>	59.6	0.150	3.44
PbO/SNZ	81.9	0.167	3.09
ZnO/SNZ	58.5	0.147	3.58

<sup>a</sup> Gea et al. [21]

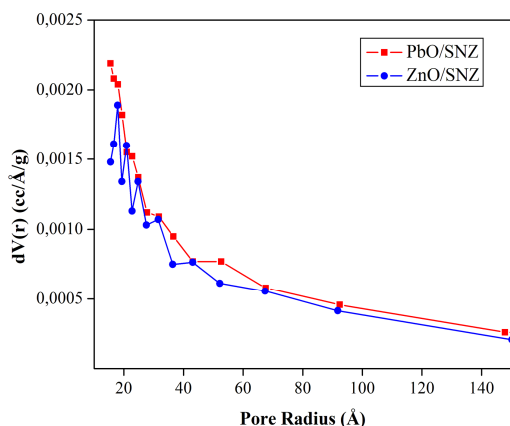


**Figure 5:** Pore size distribution of PbO/SNZ and ZnO/SNZ catalysts

### 3.6 Hydrocracking of POME

The activity test of each catalyst was carried out on the POME hydrocracking reaction. This process is carried out using a fixed bed system reactor with  $H_2$  gas flow at a temperature of  $500\text{ }^\circ\text{C}$ . Based on the characterization carried out, including Si/Al ratio, surface area, and pore characteristics, it was observed that the metal oxide-loaded zeolite had better characteristics than the basic zeolite without metal oxide. Therefore, the activity test was only carried out using PbO/SNZ and ZnO/SNZ catalysts. The catalyst mass was varied at 0.09, 0.12, and 0.15 wt.%. The resulting products are grouped into liquid, gas, coke, and heavy oil residues. The distribution of POME hydrocracking products catalyzed by each catalyst is shown in Figure 6.

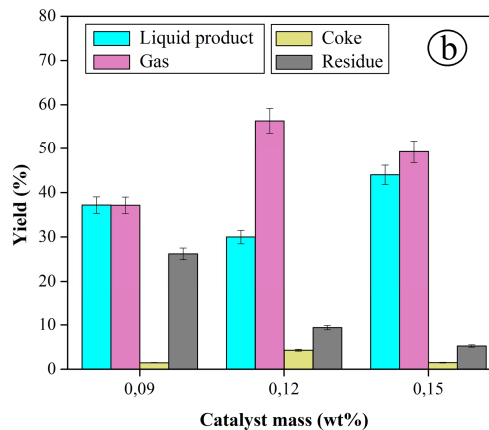
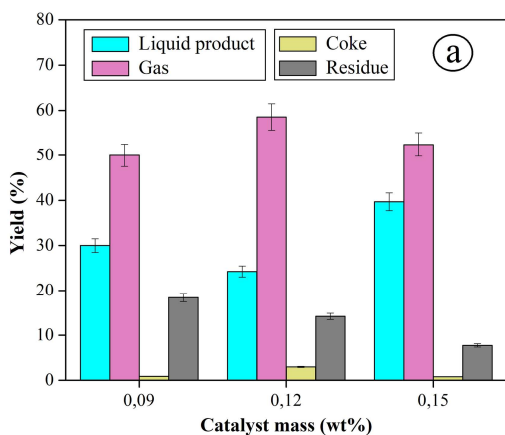


**Figure 6:** Distribution of POME hydrocracking products using (a) PbO/SNZ and (b) ZnO/SNZ catalysts with the catalyst mass of 0.09, 0.12, and 0.15 wt.%

Based on the product distribution data in Figure 6, the yield of liquid and gas products produced from hydrocracking POME using both catalysts with various ratios shows a fairly similar trend. The difference in yield produced in this case is related to the amount of catalyst used to add active sites that play a role during the hydrocracking process [38,39]. In general, the most liquid product of 40-44% is obtained from POME catalyzed by both catalysts with a mass of 0.15 wt.%. Meanwhile, the highest product gas produced was 56-59% at a catalyst mass of 0.12 wt.%. These results indicate that the amount of catalyst used has an effect on the resulting liquid and gas products. When the catalyst used was only 0.09 wt.%, there was still a lot of residue left unconverted, and the amount of this residue gradually decreased with the increase in the amount of catalyst used. These results indicate that the catalyst mass of 0.09 wt.% is not enough to convert all the reactants. Although the product is desorbed from the active site, the amount of reactants that is very large compared to the amount of catalyst can interfere with the absorption process on the active site of the catalyst.

On the other hand, the number of active sites to assist the catalytic process also has an impact on the formation of coke [40]. The ZnO/SNZ catalyst showed the most coke formation at a mass of 0.12 wt.%. These results indicate the tendency of the catalyst to produce better products but is accompanied by the formation of coke on the catalyst. This assumption is correlated with pore size data which shows that the pore diameter of the

ZnO/SNZ catalyst is the largest, therefore the catalytic process for bulk molecules can be facilitated. Coke is formed from aromatic hydrocarbons through polymerization and aromatization reactions which produce a fairly high coke yield [41]. On the other hand, in the PbO/SNZ catalyst, the gas product is significantly correlated with a narrower pore size, thus tending to convert smaller molecules.

### 3.7 Selectivity of Biofuel Fraction

The hydrocracking process using metal oxides catalyst embedded in active natural zeolite is expected to cut heavy molecular compounds contained in oil extracted from POME into lighter biofuel molecules. The liquid products produced during this catalytic process are classified into several fuel fractions, including gasoline (C5-C11), kerosene (C12-C15), and diesel fractions (C14-C20). The selectivity of liquid products in the fuel fraction is shown in Figure 7.

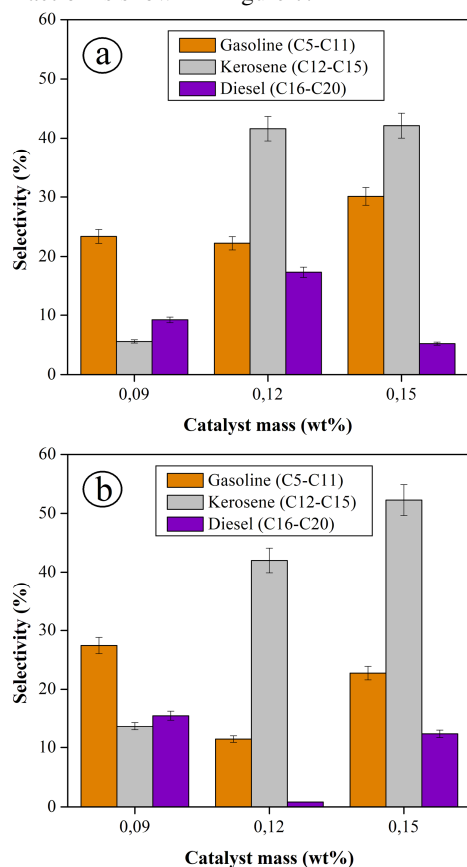


**Figure 7:** Selectivity of liquid products to gasoline, kerosene, and diesel fractions using (a) PbO/SNZ and (b) ZnO/SNZ catalysts with the catalyst mass of 0.09, 0.12, and 0.15 wt. %

Based on the previous data in Table 1, extracted oil from POME content is dominated by the diesel fraction (C16-C20). After undergoing the hydrocracking process, large molecules break up into smaller molecules which result in a significant increase in the content of gasoline and kerosene fractions. On the other hand, the content of heavy oil and diesel fractions was drastically reduced. PbO/SNZ catalyst showed better selectivity for lighter fuel fractions. The liquid product catalyzed by PbO/SNZ was more selective towards the gasoline fraction with selectivity of 22-30%. Meanwhile, the ZnO/SNZ catalyst produced more kerosene fraction with the highest selectivity of 52% at a mass of 0.15 wt. %.

Based on the report of Hasanudin et al.[42], the hydrocracking reaction of oil begins with the breakdown of glycerol ester bonds from fatty acids into free fatty acids. Kerosene is produced when hydrogenation takes place. Simultaneously, the decarboxylation reaction is initiated by the adsorption of fatty acids on the catalyst surface, which is achieved through the adsorption of oxygen atoms with the carboxyl groups of the fatty acids. As a result, the kerosene fraction is produced in high quantities. Further hydrocracking of kerosene hydrocarbons, will produce a gasoline fraction. However, in the case of ZnO/SNZ catalyst, the relatively large amount of kerosene production is not balanced enough with further conversion to gasoline fraction due to the ease with which this catalyst is deactivated due to coke formation. The proposed reaction mechanism for hydrocracking of the highest fatty acid components (palmitic acid and linoleic acid) is shown in Figure 8.

Based on Figure 8, at the initial stage, the linoleic acid contained in the feed will undergo a hydrogenation reaction. This reaction results in the addition of hydrogen (H<sub>2</sub>) where H<sup>+</sup> will attack the C=C bond present in the linoleic acid compound to form oleic acid. The oleic acid then undergoes further hydrogenation to form stearic acid [43,44]. Stearic acid and palmitic acid, which are saturated chains, experience hydrodeoxygenation which releases their hydroxyl groups as water molecules to form aldehydes (octadecanal and hexadecanal). These aldehydes will be converted to form alcohol compounds through dehydrogenation which will then undergo dehydration to form alkene compounds (octadecene and hexadecene) [45]. The

resulting alkene will undergo another hydrogenation reaction to produce an alkane. Finally, these alkane compounds can be broken down into lighter alkane fractions, such as Undecane and Heptane [46]. The most dominant alkane product produced according to GC-MS data is Heptadecane, which goes through decarboxylation and decarbonylation pathways. These results prove that the decarboxylation and decarbonylation pathways are the preferred pathways for the fatty acid cracking process from POME residues.

The ability of a catalyst to catalyze a reaction is related to the characteristics of the material. The superiority of the ZnO/SNZ catalyst is supported by its flat morphology with homogeneous particles, as well as its fairly large pore diameter. These material properties encourage the absorption of bulk molecules with a larger size to experience chain breakage during the hydrocracking reaction. This has an impact on increasing the conversion rate of heavy molecules into light fractions. Meanwhile, the advantages of PbO/SNZ catalysts is supported by its large surface area to bind reactant molecules on the catalyst surface during the catalytic reaction. In addition, it is also correlated with mapping imaging data which shows the presence of Pb elements widely scattered on the surface of the zeolite, which can add to the active sites involved during the reaction on the catalyst surface. The active site that adsorbs hydrogen atoms from H<sub>2</sub> gas is then transferred into the compound to be broken down and will eventually be replaced with hydrocarbon molecules through a cracking reaction catalyzed by the Bronsted acid site on the catalyst. Therefore, the more availability active site, the more effective the hydrocracking reaction.

### 3.8 Calorific Value of Biofuel Products

The higher heating value (HHV) of the liquid product resulting from the hydrocracking catalytic reaction was further analyzed using a bomb calorimeter. The data obtained are summarized in Table 4.

**Table 4**  
The calorific value of liquid products

Sample	HHV (MJ/kg)
Oil extracted from POME	39.4
PbO/SNZ 0.09 wt. %	43.5
PbO/SNZ 0.12 wt. %	42.3

PbO/SNZ 0.15 wt. %	43.6
ZnO/SNZ 0.09 wt. %	43.3
ZnO/SNZ 0.12 wt. %	44.2
ZnO/SNZ 0.15 wt. %	43.9

Based on the data in Table 4, there was an increase in HHV after the hydrocracking process. The increase that occurs varies between 7-12% of the initial HHV value of oil extracted from POME. The highest biofuel calorific value of 44.2 MJ/kg was obtained from the liquid product catalyzed by ZnO/SNZ 0.12 wt.%, while the lowest was 42.3 MJ/kg catalyzed by PbO/SNZ 0.12 wt.%.

## 4. Conclusion

The conversion of residual oil from POME into biofuel has been carried out through the hydrocracking method using a fixed bed reactor system. The obtained biofuels have the highest conversion rate to liquid products of 40-44% obtained from POME catalyzed by all catalysts with a catalyst mass of 0.15 wt.%. Meanwhile, the maximum amount of gas produced is 56-59% at a catalyst mass of 0.12 wt.%. The liquid product catalyzed by PbO/SNZ was more selective towards the gasoline fraction with selectivity of 22-30%. Meanwhile, 0.15 wt.% ZnO/SNZ catalyst produced more kerosene fraction with the highest selectivity of 52%. The activity of PbO/SNZ catalyst is supported by its large surface area to bind reaction molecules to the catalyst during the catalytic reaction. Meanwhile, the activity of ZnO/SNZ catalyst is supported by its homogeneous morphology with fine particles, as well as larger pore diameters that encourage the absorption of bulk molecules to undergo chain breakage during the hydrocracking reaction. The HHV of the hydrocracking liquid product increased by 7-12%. The highest HHV of 44.2 MJ/kg was obtained from the liquid product catalyzed by ZnO/SNZ 0.12 wt.%.

## CRedit authorship contribution statement

**Gimelliya Saragih:** Conceptualization, Methodology, Data curation, Writing-original draft, Supervision. **Harmileni:** Formal analysis, Writing-original draft, Supervision. **Junifa Layla Sihombing:** Conceptualization, Supervision, Visualization, Writing- original draft. **Ahmad Nasir Pulungan:** Methodology, Supervision, Data curation, Writing- review & editing.

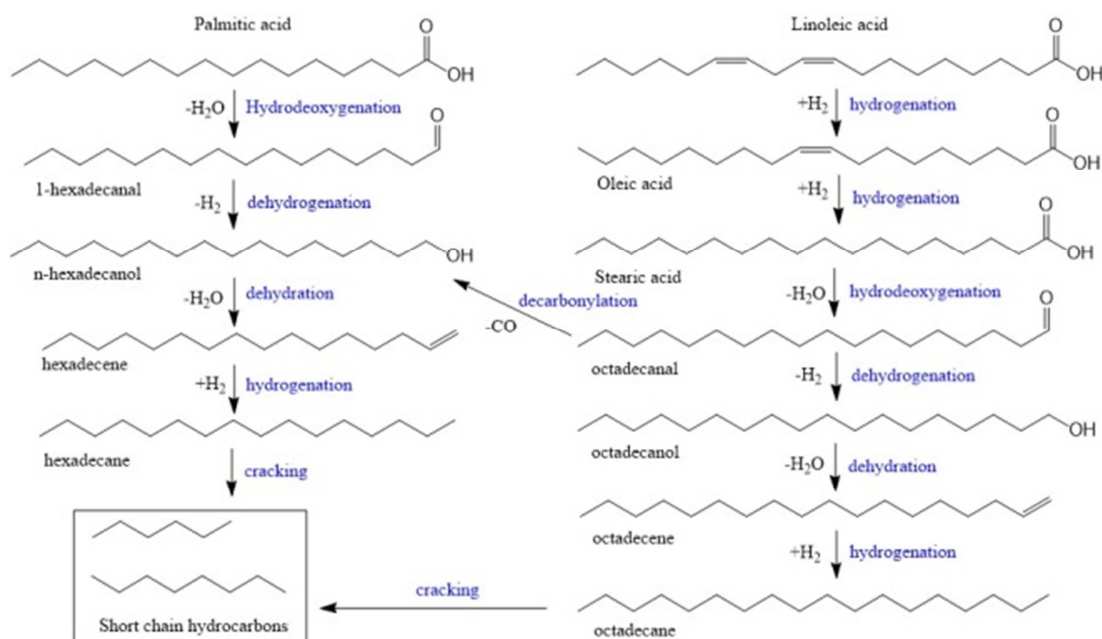


**Figure 8:** The proposed mechanism pathway for the transformation of linoleic acid and palmitic acid

### Conflicts of interest

The authors declare that they have no known competing financial interests or personal relationships that could have appeared to influence the work reported in this paper.

### Acknowledgments

The author would like to acknowledge the Industrial Human Resources Development Agency (BPSDM) of the Indonesian Ministry of Industry and Politeknik Teknologi Kimia Industri Medan.

### 5. References

- [1] Chaijak P, Sukkasem C, Lertworapreecha M, Boonsawang P, Wijasika S. Enhancing Electricity Generation Using a Laccase-Based Microbial Fuel Cell with Yeast *Galactomyces reessii* on the Cathode. *J Microbiol Biotechnol* 2018;28:1360–6. <https://doi.org/10.4014/jmb.1803.03015>.
- [2] Lam S-M, Wong K-A, Sin J-C. Fabrication of Flower-like ZnO Micro/Nanostructures for Photodegradation of Pre-treated Palm Oil Mill Effluent. *IOP Conf Ser Earth Environ Sci* 2018;112:12003. <https://doi.org/10.1088/1755-1315/112/1/012003>.
- [3] Subramaniam MN, Goh PS, Lau WJ, Ng BC, Ismail AF. AT-POME colour removal through photocatalytic submerged filtration using antifouling PVDF-TNT nanocomposite membrane. *Sep Purif Technol* 2018;191:266–75. <https://doi.org/https://doi.org/10.1016/j.seppur.2017.09.042>.
- [4] Bello MM, Abdul Raman AA. Trend and current practices of palm oil mill effluent polishing: Application of advanced oxidation processes and their future perspectives. *J Environ Manage* 2017;198:170–82. <https://doi.org/https://doi.org/10.1016/j.jenvman.2017.04.050>.
- [5] Ahmed Y, Yaakob Z, Akhtar P, Sopian K. Production of biogas and performance evaluation of existing treatment processes in palm oil mill effluent (POME). *Renew Sustain Energy Rev* 2015;42:1260–78. <https://doi.org/https://doi.org/10.1016/j.rser.2014.10.073>.
- [6] Onoja E, Chandren S, Abdul Razak FI, Mahat NA, Wahab RA. Oil Palm (*Elaeis guineensis*) Biomass in Malaysia: The Present and Future Prospects. *Waste and Biomass Valorization* 2019;10:2099–117. <https://doi.org/10.1007/s12649-018-0258-1>.
- [7] Hadiyanto H, Azimatun Nur MM, Hartanto GD. Cultivation of *Chlorella* sp. as biofuel sources in palm oil mill effluent (POME). *Int J Renew Energy Dev* 2012;1:45–9. <https://doi.org/10.14710/ijred.1.2.45-49>.
- [8] Ahmad A, Buang A, Bhat AH. Renewable and sustainable bioenergy production from

- microalgal co-cultivation with palm oil mill effluent (POME): A review. *Renew Sustain Energy Rev* 2016;65:214–34. <https://doi.org/https://doi.org/10.1016/j.rser.2016.06.084>
- [9] Hosseini SE, Bagheri G, Khaleghi M, Abdul Wahid M. Combustion of Biogas Released from Palm Oil Mill Effluent and the Effects of Hydrogen Enrichment on the Characteristics of the Biogas Flame. *J Combust* 2015;2015:612341. <https://doi.org/https://doi.org/10.1155/2015/612341>.
- [10] Klabsong M, Kungskulniti N, Puemchalad C, Charoencan N, Punsuvon V. Feasibility study of biodiesel production from residual oil of palm oil mill effluent. *Int J GEOMATE* 2017;12:60–4. <https://doi.org/10.21660/2017.33.2568>.
- [11] Hing Chung C, Janaun J, Semilin V, Sinan Balan W. Recovery of Residual Oil From Palm Oil Mill Effluent Using Polypropylene Nanofiber: a Field Trial. *MATTER Int J Sci Technol* 2017;3:276–94. <https://doi.org/10.20319/mijst.2017.32.276294>.
- [12] Sundaryono A, Firdaus ML, Latifah N, Listiono AE. Development of a Learning Module Based on Biofuel Synthesis Laboratory Research from CPO Residual of Palm Oil Mill Effluent (POME) with Ultrasonic Irradiation Assistance BT - Proceedings of the International Conference on Educational Sciences and Teacher, Atlantis Press; 2019, p. 239–43. <https://doi.org/https://doi.org/10.2991/icetep-18.2019.57>.
- [13] Said M, Mohammad AW, Nor MTM, Abdullah SRS, Hasan HA. Investigation of three pre-treatment methods prior to nanofiltration membrane for palm oil mill effluent treatment. *Sains Malaysiana* 2015;44:421–7. <https://doi.org/10.17576/jsm-2015-4403-14>.
- [14] Alrawi RA, Ab Rahman NNN, Ahmad A, Ismail N, Mohd Omar AK. Characterization of Oily and Non-Oily Natural Sediments in Palm Oil Mill Effluent. *J Chem* 2013;2013:298958. <https://doi.org/10.1155/2013/298958>.
- [15] Sihombing JL, Gea S, Pulungan AN, Agusnar H, Wirjosentono B, Hutapea YA. The characterization of Sarulla natural zeolite crystal and its morphological structure. *AIP Conf Proc* 2018;2049. <https://doi.org/10.1063/1.5082467>.
- [16] Patil SJ, Vaidya PD. Production of Hydrotreated Jatropa Oil Using Co–Mo and Ni–Mo Catalysts and Its Blending with Petroleum Diesel. *Energy & Fuels* 2018;32:1812–21. <https://doi.org/10.1021/acs.energyfuels.7b03305>.
- [17] Hanafi SA, Elmelawy MS, Shalaby NH, El-Syed HA, Eshaq G, Mostafa MS. Hydrocracking of waste chicken fat as a cost effective feedstock for renewable fuel production: A kinetic study. *Egypt J Pet* 2016;25:531–7. <https://doi.org/https://doi.org/10.1016/j.ejpe.2015.11.006>.
- [18] Zaher F, Gad MS, Aly SM, Hamed SF, Abo-Elwafa GA, Zahran HA. Catalytic cracking of vegetable oils for producing biofuel. *Egypt J Chem* 2017;60:291–300. <https://doi.org/10.21608/ejchem.2017.2967>.
- [19] Kumar P, Maity SK, Shee D. Role of NiMo Alloy and Ni Species in the Performance of NiMo/Alumina Catalysts for Hydrodeoxygenation of Stearic Acid: A Kinetic Study. *ACS Omega* 2019;4:2833–43. <https://doi.org/10.1021/acsomega.8b03592>.
- [20] Patil SJ, Vaidya PD. On the Production of Bio-Hydrogenated Diesel over Hydrotalcite-like Supported Palladium and Ruthenium Catalysts. *Fuel Process Technol* 2018;169:142.
- [21] Fatimah I, Rubiyanto D, Yudha SP. Effect of KF modification to kaolinite catalytic activity in microwave-assisted biodiesel conversion. *Egypt J Chem* 2018;61:213–23. <https://doi.org/10.21608/ejchem.2018.2041.1163>.
- [22] Negm NA, Sayed GH, Yehia FZ, Dimitry OIH, Rabie AM, Azmy EAM. Production of biodiesel production from castor oil using modified montmorillonite clay. *Egypt J Chem* 2016;59:1045–60. <https://doi.org/10.21608/ejchem.2016.1551>.
- [23] Sihombing JL, Gea S, Wirjosentono B, Agusnar H, Pulungan AN, Herlinawati H, et al. Characteristic and Catalytic Performance of Co and Co-Mo Metal Impregnated in Sarulla Natural Zeolite Catalyst for Hydrocracking of MEFA Rubber Seed Oil into Biogasoline Fraction. *Catalysts* 2020;10:121.
- [24] Husna AF, Febrianti F, Syah HH, Pangaribuan RA, Surbakti TA, Sihombing JL, et al. Conversion of Cellulose from Palm Oil Middle Waste (*Elaeis Guineensis*) into Bio-oil Products As Alternative Fuel. *Egypt J Chem* 2022;65:61–7. <https://doi.org/10.21608/ejchem.2022.96526.4517>.
- [25] Gea S, Haryono A, Andriyani A, Sihombing JL, et al. The Stabilization of Liquid Smoke through Hydrodeoxygenation Over Nickel Catalyst Loaded on Sarulla Natural Zeolite. *Appl Sci* 2020;10:1–17.
- [26] Pulungan AN, Kembaren A, Nurfajriani N, Syuhada FA, Sihombing JL, Yusuf M, et al.

- Biodiesel production from rubber seed oil using natural zeolite supported metal oxide catalysts. *Polish J Environ Stud* 2021;30:5681–9. <https://doi.org/10.15244/pjoes/135615>.
- [27] Hasanudin H, Putri QU, Agustina TE, Hadiyah F. Esterification of Free Fatty Acid in Palm Oil Mill Effluent usSulfated Carbon-Zeolite Composite Catalyst. *Pertanika J Sci Technol* 2022;30:377–95. <https://doi.org/10.47836/pjst.30.1.21>.
- [28] Muanruksa P, Winterburn J, Kaewkannetra P. Biojet Fuel Production from Waste of Palm Oil Mill Effluent through Enzymatic Hydrolysis and Decarboxylation. *Catalysts* 2021;11. <https://doi.org/10.3390/catal11010078>.
- [29] Tang YM, Wong WY, Tan KT, Wong LP. Enhanced oil recovery from palm oil mill effluent using ultrasonication technique. *IOP Conf Ser Earth Environ Sci* 2021;945:12042. <https://doi.org/10.1088/1755-1315/945/1/012042>.
- [30] Wahyuni ET, Diantariani NP, Kartini I, Kuncaka A. Enhancement of the photostability and visible photoactivity of ZnO photocatalyst used for reduction of Cr(VI) ions. *Results Eng* 2022;13:100351. <https://doi.org/https://doi.org/10.1016/j.rineng.2022.100351>.
- [31] Borhade A V., Tope DR, Uphade BK. An efficient photocatalytic degradation of methyl blue dye by using synthesised PbO nanoparticles. *E-Journal Chem* 2012;9:705–15. <https://doi.org/10.1155/2012/362680>.
- [32] Park JH, Sin KS, Chang S, Park SH, Cho SJ. Structural analysis of Cu/Zeolite with controlled Si/Al ratio and the resulting thermal stability. *Catal Today* 2022. <https://doi.org/https://doi.org/10.1016/j.cattod.2022.08.008>.
- [33] Li Q, Wu Z, Tu B, Park SS, Ha C-S, Zhao D. Highly hydrothermal stability of ordered mesoporous aluminosilicates Al-SBA-15 with high Si/Al ratio. *Microporous Mesoporous Mater* 2010;135:95–104. <https://doi.org/https://doi.org/10.1016/j.micro-meso.2010.06.016>.
- [34] Gea S, Irvan, Wijaya K, Nadia A, Pulungan AN, Sihombing JL, et al. Bio-oil hydrodeoxygenation over zeolite-based catalyst: the effect of zeolite activation and nickel loading on product characteristics. *Int J Energy Environ Eng* 2022;13:541–53. <https://doi.org/10.1007/s40095-021-00467-0>.
- [35] Gea S, Irvan I, Wijaya K, Nadia A, Pulungan AN, Sihombing JL, et al. Bio-oil hydrodeoxygenation over acid activated-zeolite with different Si/Al ratio. *Biofuel Res J* 2022;9:1630–9. <https://doi.org/10.18331/brj2022.9.2.4>.
- [36] Medeiros-Costa IC, Laroche C, Coasne B, Pérez-Pellitero J. Xylene Selectivity at the External Surface of Hierarchical Zeolites: Experiment and Molecular Modeling. *Ind Eng Chem Res* 2022;61:10184–94. <https://doi.org/10.1021/acs.iecr.2c00791>.
- [37] Hu S, Jia H, Ma J, Hao W, Li R. A hierarchical zeolite microsphere prepared by an eco-friendly and practical route for efficient reaction of bulky molecules. *Microporous Mesoporous Mater* 2020;294:109931. <https://doi.org/https://doi.org/10.1016/j.micro-meso.2019.109931>.
- [38] Sankaranarayanan TM, Berenguer A, Ochoa-Hernández C, Moreno I, Jana P, Coronado JM, et al. Hydrodeoxygenation of anisole as bio-oil model compound over supported Ni and Co catalysts: Effect of metal and support properties. *Catal Today* 2015;243:163–72. <https://doi.org/10.1016/j.cattod.2014.09.004>.
- [39] Roldugina EA, Naranov ER, Maximov AL, Karakhanov EA. Hydrodeoxygenation of guaiacol as a model compound of bio-oil in methanol over mesoporous noble metal catalysts. *Appl Catal A Gen* 2018;553:24–35. <https://doi.org/10.1016/j.apcata.2018.01.008>.
- [40] Nava R, Pawelec B, Castaño P, Álvarez-Galván MC, Loricera C V., Fierro JLG. Upgrading of bio-liquids on different mesoporous silica-supported CoMo catalysts. *Appl Catal B Environ* 2009;92:154–67. <https://doi.org/10.1016/j.apcatb.2009.07.014>.
- [41] Sangdara P, Subsadsana M, Ruangviriyachai C. Liquid biofuel production from palm oil using dual-function of Zn/HZSM-5 catalyst. *Orient J Chem* 2017;33:2257–62. <https://doi.org/10.13005/ojc/330513>.
- [42] Hasanudin H, Asri WR, Putri QU, Fanani Z, Agustina TE, Wijaya K. Montmorillonite-Zirconium Phosphate Catalysts for Methanol Dehydration. *Iran J Catal* 2022;12:389–97. <https://doi.org/10.30495/IJC.2022.1960655.1942>.
- [43] Falabella Sousa-Aguiar E, Zanon Costa C, Peixoto Gimenes Couto MA, de Almeida Azevedo D, Filho JFS de C. Conversion of residual palm oil into green diesel and biokerosene fuels under sub-and supercritical conditions employing raney nickel as catalyst. *Catalysts* 2021;11. <https://doi.org/10.3390/catal11080995>.
- [44] Puello-Polo E, Arias D, Márquez E. Al<sub>2</sub>O<sub>3</sub>-MgO Supported Ni, Mo, and NiMo Mixed Phosphidic-Sulphidic Phase for Hydrotreating of Stearic and Oleic Acids Into Green Diesel.

- Front Chem 2022;10:1–18.  
<https://doi.org/10.3389/fchem.2022.880051>.
- [45] Duongbia N, Kannari N, Sato K, Takarada T, Chaiklangmuang S. Production of bio-based chemicals from palmitic acid by catalytic hydrotreating over low-cost Ni/LY char and limonite catalysts. Alexandria Eng J 2022;61:3105–24.  
<https://doi.org/10.1016/j.aej.2021.08.037>.
- [46] Konwar LJ, Oliani B, Samikannu A, Canu P, Mikkola JP. Efficient hydrothermal deoxygenation of tall oil fatty acids into n-paraffinic hydrocarbons and alcohols in the presence of aqueous formic acid. Biomass Convers Biorefinery 2022;12:51–62.  
<https://doi.org/10.1007/s13399-020-01103-3>.